Hindawi
Advances in Civil Engineering
Volume 2020, Article ID 6520982, 11 pages
https://doi.org/10.1155/2020/6520982

Research Article

Experimental Research on Seismic Performance of Damaged Brick Walls Strengthened with Embedded Horizontal Steel Bars

Liu Tingbin,[1,2] **Jia Rubo**,[2] **Pei Xianke**,[3] **Zhang Jiawei**,[2] **and Zhao Jianchang**[2]

[1]*Key Laboratory of Road & Bridges and Underground Engineering of Gansu Province, Lanzhou Jiaotong University, Lanzhou, China*
[2]*National and Provincial Joint Engineering Laboratory of Road & Bridge Disaster Prevention and Control, Lanzhou Jiaotong University, Lanzhou, China*
[3]*Gansu Building Materials Design & Research Institute Co., Ltd., Lanzhou, China*

Correspondence should be addressed to Liu Tingbin; liutingbin1203@163.com and Zhao Jianchang; zhaojchang@163.com

Received 28 June 2019; Revised 8 November 2019; Accepted 19 November 2019; Published 10 February 2020

Academic Editor: Flora Faleschini

Six brick masonry specimens (two unreinforced specimens, two reinforced specimens, and two specimens reinforced after being damaged), which have different aspect ratios, were tested under low-frequency cyclic loading. The seismic performances of these specimens, including failure characteristics, deformation capacity, carrying capacity, energy dissipation capacity, hysteresis characteristics, and stiffness degradation, were analyzed. The following results were obtained: the ductility of the damaged walls could be significantly improved after they were reinforced with embedded horizontal steel bars; the ultimate shear capacity of the damaged brick masonry walls with the aspect ratios of 1.8 and 0.5 was improved by 6.8% and 4.7%, respectively; the displacement corresponding to the ultimate bearing capacity was close to that of the unreinforced brick masonry wall; the hysteresis loop of the reinforced wall became plumper and encompassed a larger area; after the ultimate load was reached, a clear yielding platform appeared in the skeleton curve of the reinforced wall; the reinforced wall exhibited good ductility, after entering plastic stage; the energy dissipation capacity of the reinforced wall was significantly greater than that of the unreinforced wall. In conclusion, the seismic performance of the damaged brick masonry wall can be improved by embedding horizontal steel bars, and this reinforcing method can be applied in the postseismic reconstruction process.

1. Introduction

The last two decades have witnessed mass casualties, heavy property loss, and severe damage to engineering structures caused by violent earthquakes. Seismic events in Chile [1], China [2], Haiti [3, 4], Nepal [5], Indonesia [6], Iran [7], and Europe [8] damaged or even demolished thousands of masonry structures. A main cause for casualties in the earthquakes is that a large number of unreinforced brick masonry structures (URM) still exist around the world. In the postdisaster recovery and reconstruction stage, economic and reliable restoration methods are generally needed to speed up the postdisaster reconstruction process.

Various reinforcement methods are given in the design codes in different countries aiming at the reinforcement of damaged brick masonry structures [9–11], such as surface fiber reinforcement (FRP, BFRP, NSM-FRP, etc.) [12–14], joint reinforcement [15], steel reinforcement [16], and textile-mortar reinforcement [17]. For these reinforcement methods, a lot of research work has been carried out.

In the area of masonry reinforcement, another interesting and relatively new technique used to repair brick or stone masonry is insertion of twisted stainless steel bars [18, 19] or CFRP strips [20] in horizontal joints, the purpose of which is to form enclosing loop to restrain the unreinforced masonry walls.

For this type of technique, after slots (20–60 mm deep) are cut in the original joints, the steel bars or CFRP strips are inserted and then mortar is pasted. This allows preserving

the fair-faced aspect of the masonry wall, without changing its original appearance, as the longitudinal bars are embedded with new mortar into the existing horizontal joints. Typically, longitudinal steel bars on both sides of the wall are tied by transverse steel bars. When the thickness of the walls is too large to bore and permit the transverse bars to pass through, the connection can be made with transverse bars, which run about 2/3 as long as the thickness of the wall and are anchored by injecting non-shrink high-strength mortar. Finally, a surface layer of new mortar, which completely covers the longitudinal bars, makes the reinforcement completely invisible and preserves the fair-faced aspect of the masonry.

This retrofitting technique has been the subject of study of several researchers. The overall effectiveness of the method was studied by Ismail and Ingham [21], who find that through the reinforcing, not only the strength is increased about 434%, compared to the unreinforced walls, but also the ductility capacity of the walls is largely increased. Moreira et al. [22] tested the pull-out behaviour of twisted stainless steel bars in mortar joints, demonstrating the high bonding characteristics of the bars in mortar. Recently, Petersen et al. [23] proposed a method for a finite element modelling of unreinforced masonry walls strengthened with twisted steel bars, providing a valuable method for design purpose.

In this paper, damaged brick masonry walls are chosen and hot-rolled plain steel bars are embedded in the walls, which is different from other researches. Experimental research on seismic performance of damaged brick walls strengthened with embedded horizontal steel bars was performed. The pseudostatic tests of six specimens of brick masonry walls, with different aspect ratios, were carried out under the action of low-frequency cyclic loading. The failure characteristics, carrying capacity, deformation capacity, energy dissipation capacity, hysteresis characteristics, and other seismic performances of unreinforced brick masonry walls, undamaged brick masonry walls reinforced by embedded bars, and damaged brick masonry walls reinforced by embedded bars were analyzed, respectively, and compared.

2. Testing Conditions

2.1. Specimen Design. The standard clay brick with a size of 240 mm × 115 mm × 53 mm was adopted, and its strength grade was MU7.5 (GB/T 2542-2012 [24]). M2.5 grade composite mortar was selected as the masonry mortar. The caulking material is YS-JGF (GB50728-2011 [25]), and it is produced by the Gansu Institute of Civil Engineering Science. The grade for the steel bars is HPB300 (GB1499.1-2008 [26]). The performance indexes of the caulking cement and steel bar are shown in Tables 1 and 2, respectively. According to GB/T50129-2011 [27], the measured shear strength f_{v0} and compressive strength f of the masonry were 0.19 MPa and 1.8 MPa, respectively.

Considering the loading capacity of testing equipment and the size of the wall piers between openings, the aspect ratios of specimens in the testing were chosen to be 1.8 and 0.5, respectively. The geometry size and reinforcement of the specimen are shown in Figure 1. The brick walls were built on reinforced concrete base beams. The first layer of brick and the base beam were bonded with high-strength mortar to ensure that there was no sliding between the wall and the base beam during the horizontal loading process. The thickness of the mortar joint was controlled between 10 mm and 12 mm during the construction. After cured for 28 days, the wall, together with the base beam, was hoisted to the test platform and was fixed to the test platform by ground anchoring bolts. The specimens Q1 and Q2 were unreinforced brick masonry specimens; the specimens QA1 and QA2 were reinforced specimens before damaging; the specimens JQ1 and JQ2 were reinforced Q1 and Q2 specimens, which had undergone some damage, in advance, under the action of low-frequency cyclic loading. The basic parameters of the specimens and the vertical loading values are shown in Table 3.

2.2. Reinforcement Scheme. Horizontal slots, which are 30 mm deep and 12 mm wide, were cut, every 4 layers of brick and along the horizontal mortar joint, into the masonry, on every vertical plane of the specimen. The dust produced in the cutting process was cleaned, and the cut slots were moistened. The cement paste was painted, and the cement gum was embedded to half depth of the slots. Longitudinal steel bars were embedded in the slots and tied by transverse steel bars, with an interval of 300 mm along the specimen. Finally, the cement gum was pressed into mortar slots, and the pointing was completed.

To ensure safety in the reinforcement process, 4 L20 × 4 steel angles and steel bars with a diameter of 16 mm were used to constrain the damaged specimen, as shown in Figure 2(a). After the severely damaged bricks were removed, the caulking cement was injected into the cavity left, and some small cracks were sealed and repaired with 1 : 1 gluing cement paste. After the gluing cement became hardened, the temporary constraints of the specimen were removed. The specimen was strengthened according to the reinforcement method before damaged, as shown in Figures 2(b) and 2(c). The reinforced specimens were cured for 28 days.

2.3. Loading Device of Tests. The specimens were tested according to the method described in JGJ101-2015 [28]. As shown in Figure 3, the vertical axial force was applied to the specimen by a hydraulic jack (with the maximum load being 3000 kN), with the steel frame beam as the reaction force support, and the vertical load kept constant throughout the testing process. As shown in Figure 4 (in the figure, P_{cr} is the test values of cracking load; Δ_{cr} is the displacement corresponding to cracking load), the horizontal force was applied by an hydraulic servo loading system (with the maximum load being 300 kN). A load-displacement double-control loading program was adopted. Load control was implemented before the specimen reached the estimated limit load, and the loading increment was reduced when close to

Table 1: Mechanical performance indexes of steel bar.

Specification	Diameter D (mm)	Area A_s (mm^2)	Yield strength f_y (MPa)	Ultimate strength f_t (MPa)	Elastic modulus E_s (MPa)
HPB300	6.5	33.2	315	420	2.10×10^5

Table 2: Performance indexes of caulking cement.

Specification	Compressive strength 28 d (MPa)	Flexural strength 28 d (MPa)	Bond strength 28 d (MPa)	Grip force (MPa)
YS-JGF	50	5.5	1.8	3.0

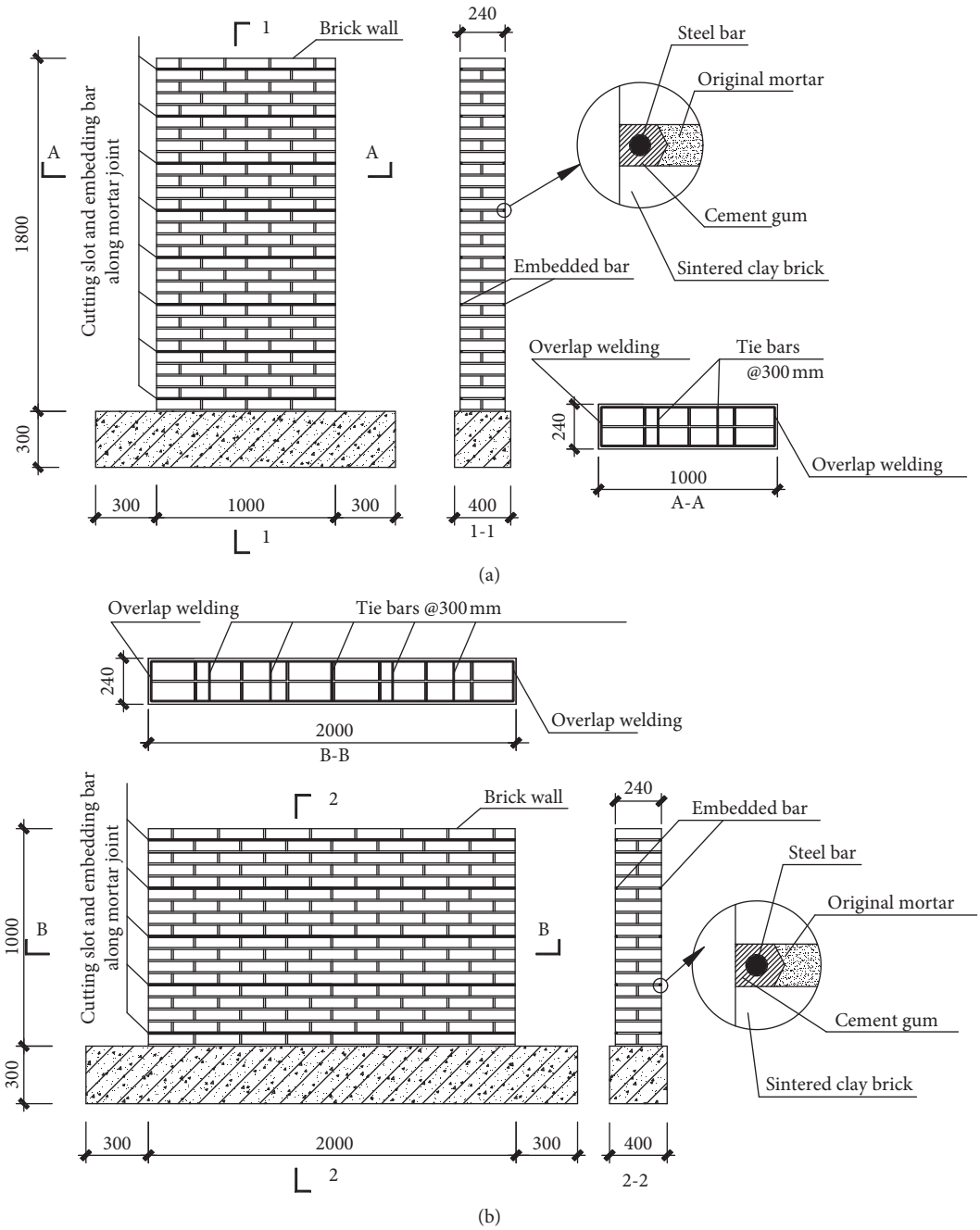

Figure 1: Geometry size and reinforcement of the specimens. (a) Geometry size and reinforcement of the specimen with aspect ratio of 1.80. (b) Geometry size and reinforcement of the specimen with aspect ratio of 0.50.

Table 3: Basic parameters of specimens.

Test number	Width B (mm)	Height H (mm)	Aspect ratio (H/B)	Vertical pressure N (kN)	Compressive stress σ (MPa)	Reinforcement ratio (%)	Notes
Q1	1000	1800	1.80	240	1.00	0	URM
Q2	2000	1000	0.50	330	0.69	0	URM
QA1	1000	1800	1.80	240	1.00	0.061	Reinforced every 4 layers of brick
QA2	2000	1000	0.50	330	0.69	0.083	Reinforced every 4 layers of brick
JQ1	1000	1800	1.80	240	1.00	0.061	Reinforced every 4 layers of brick
JQ2	2000	1000	0.50	330	0.69	0.083	Reinforced every 4 layers of brick

(a) (b) (c)

Figure 2: Reinforcing steps of damaged specimen. (a) Temporary constraints. (b) Slots on the specimen. (c) Embedding bar and pointing.

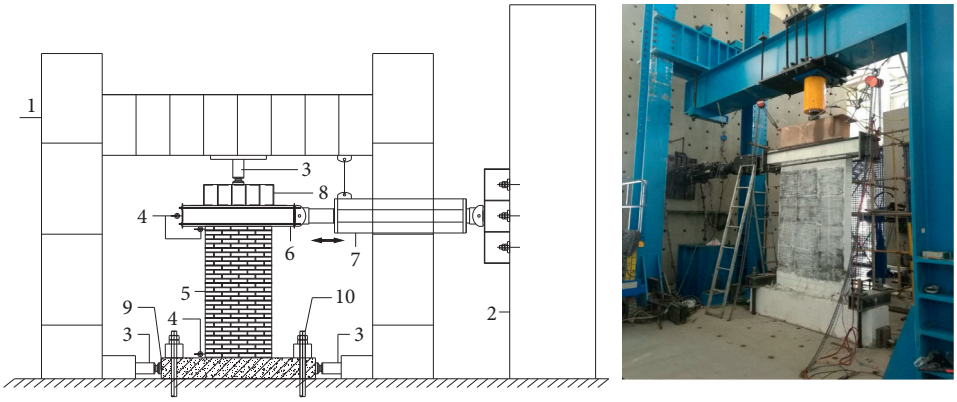

Figure 3: Diagram and real photo of testing devices. 1, reaction force frame; 2, reaction wall; 3, jacking device; 4, displacement meter; 5, specimen; 6, cap beam; 7, actuator; 8, distribution beam; 9, base beam; 10, anchoring bolt.

the limit load. After the specimen reached the limit load, the displacement control was implemented. When the load on the specimen dropped to 85% of the limit load or a large crack appeared in the specimen, it was believed that the specimen could not be further loaded and the specimen had failed.

3. Experiment Results and Analyses

3.1. Failure Modes of Specimens

3.1.1. Failure Modes of Unreinforced Specimens. For the specimen with the aspect ratio of 1.8, there were almost no indicating signs before cracks occurred. With the load reaching 82 kN, through cracks appeared promptly along the diagonal direction and developed rapidly. A large number of bricks in the diagonal direction were cut through, and the widest crack was located in the middle of the specimen, with the maximum width being about 13 mm. The failure mode is shown in Figure 5(a).

For the specimen with the aspect ratio of 0.5, when the load reached 143 kN, the crack occurred and a number of ladder-like cracks gradually developed along the mortar joint. When the load reached 180 kN, horizontal cracks appeared in the middle of the specimen, and all cracks in the corner of the specimen further extended. When the limit load was applied,

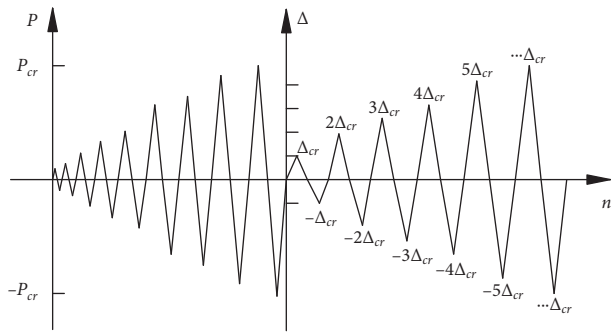

Figure 4: Horizontal loading method.

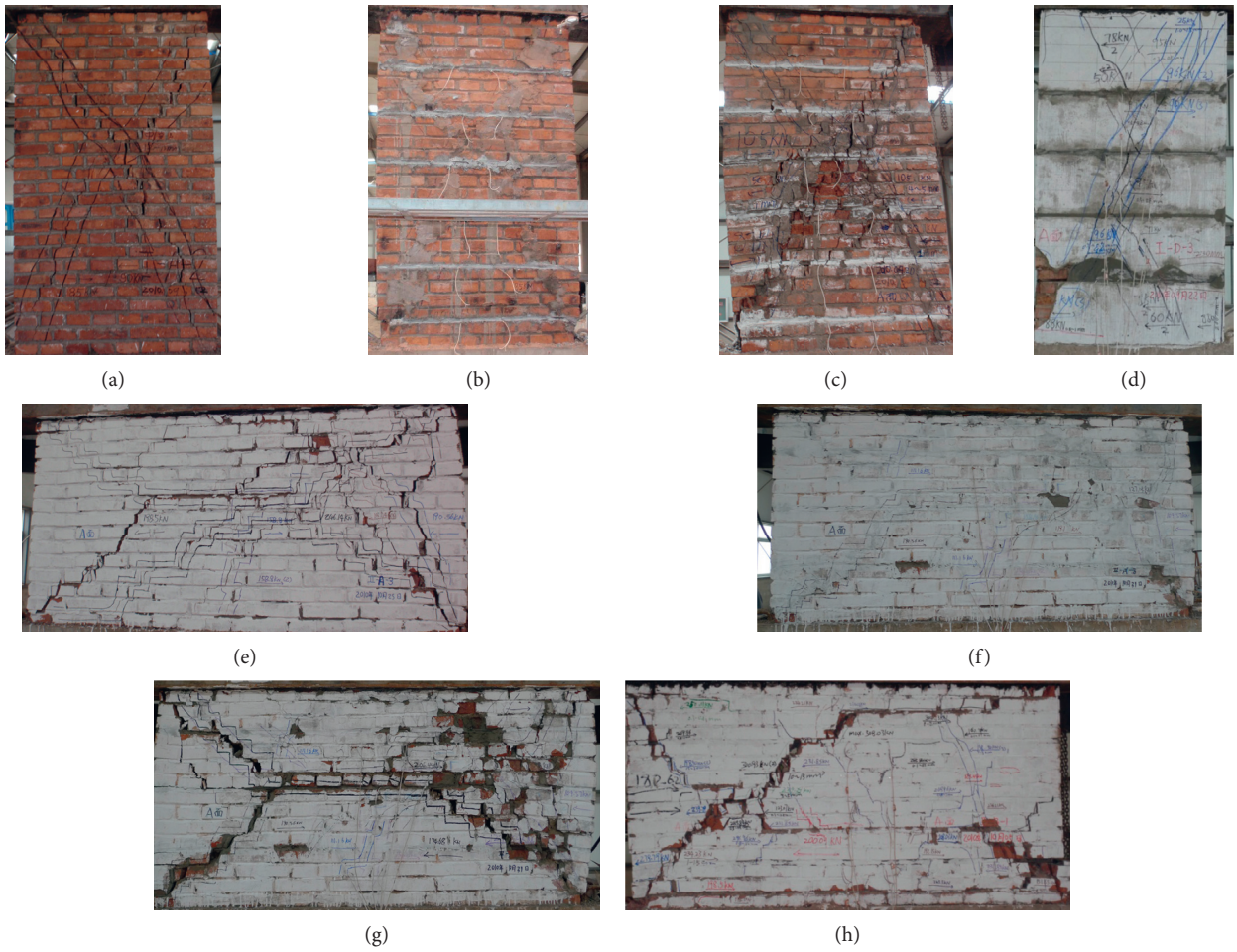

Figure 5: Failure modes of specimens. (a) Developing of cracks in Q1. (b) Morphology of Q1 after repairing (JQ1). (c) Developing of cracks in JQ1. (d) Developing of cracks in QA1. (e) Developing of cracks in Q2. (f) Morphology of Q2 after repairing (JQ2). (g) Developing of cracks in JQ2. (h) Developing of cracks in QA2.

the cracks in the corner and the middle of the specimen were basically connected, and some of the bricks were broken. The widest crack was located in the lower right corner of the specimen with the maximum width being about 15 mm, and the failure mode is shown in Figure 5(e).

3.1.2. Failure Modes of Undamaged Specimens Strengthened with Embedded Horizontal Steel Bars. For the specimen with the aspect ratio of 1.8, when the load reached 88 kN, subtle oblique cracks formed along the diagonal direction in the lower left corner and lower right corner. The cracks would further extended with the load increasing, accompanied by brittle sound during the loading process. At the same time, in other parts of the specimen, a number of oblique cracks appeared along directions parallel to the diagonal direction, and the cracks were narrow and densely distributed. When the limit load is reached, the oblique

Table 4: Shear capacity of specimens and displacement of the top surface of specimen.

Test no.	P_{cr} (kN)	κ_{cr} (%)	Δ_{cr} (mm)	δ_{cr} (%)	γ_c	P_u (kN)	κ_u (%)	Δ_u (mm)	δ_u (%)	γ_u	P_f (kN)	Δ_f (mm)	γ_f	μ
Q1	81	—	1.91	—	1/942	88	—	3.45	—	1/521	88	3.45	1/521	1.81
QA1	88	8.6	1.95	2.1	1/923	103	17.1	5.30	53.6	1/339	78	16.68	1/108	2.72
JQ1	83	—	1.86	—	1/968	94	6.8	5.07	47.0	1/197	73	15.96	1/63	—
Q2	143	—	1.73	—	1/578	190	—	6.40	—	1/156	143	15.84	1/63	3.70
QA2	152	6.3	1.83	5.8	1/546	214	12.6	7.49	17.0	1/133	168	18.53	1/54	3.86
JQ2	155	—	1.81	—	1/552	199	4.7	6.33	—1.1	1/158	155	15.65	1/64	—

cracks along the diagonal direction developed into main through cracks, and the maximum crack width was about 4 mm. The failure mode is shown in Figure 5(d).

For the specimen with the aspect ratio of 0.5, when the load reached 152 kN, horizontal cracks appeared along the mortar joints in the lower part. When the load reached 190 kN, horizontal cracks appeared along the mortar joint in the middle part, and meanwhile, the ladder-like horizontal cracks appeared along the mortar joint in the lower right corner. When the load reached 200 kN, horizontal cracks appeared in the second mortar joint from top to bottom in the top right area. With the load increasing, new oblique cracks occurred along the diagonal direction, and the original oblique cracks continued to expand and were connected with the horizontal cracks in the middle part. Finally, oblique through cracks were formed, and some bricks near the oblique cracks were broken. The failure mode was shown in Figure 5(h).

3.1.3. Failure Modes of Damaged Specimens Strengthened with Embedded Horizontal Steel Bars. The damaged specimen Q1 was renumbered as JQ1 after it was reinforced. As shown in Figure 5(b), in the initial loading process of JQ1, oblique cracks appeared immediately along the original cracking path (the diagonal direction), with the width being around 1 mm. In addition, there were almost no cracks produced in other parts. With the load increasing, cracks continued to expand slowly, and meanwhile, a number of narrow oblique cracks appeared in the direction parallel to the main crack in the middle of the specimen. The width of the main crack was about 5 mm when the specimen was failed, and the width of cracks in other parts was about 2 mm. The failure mode is shown in Figure 5(c).

The damaged specimen Q2 was renumbered as JQ2 after it was reinforced. As shown in Figure 5(f), a number of minor cracks appeared in the corner and middle of the specimen during the initial loading process. Then, many ladder-like cracks appeared on the right side of the specimen, and the original crack width increased slowly. Some of the repaired cracks on the upper right area and lower right area did not expand. The failure mode is shown in Figure 5(g).

3.2. Analysis of Failure Modes. It can be observed from the failure modes that the unreinforced specimen Q1 with the aspect ratio of 1.8 showed a typical brittle shear failure; the unreinforced specimen Q2 with the aspect ratio of 1.8 showed typical brittle shear-friction failure; the reinforced specimen QA1 with the aspect ratio of 1.8 showed typical ductile shear failure, and the reinforced specimen QA2 with the aspect ratio of 1.8 showed typical shear-friction failure with some ductility; although some cracks occurred along the original failure surface in the reinforced damaged specimens JQ1 and JQ2 during the initial loading stage, both of them still showed good ductility during the subsequent loading process. Because of the constraint effect of steel bars, all reinforced specimens exhibited a "crack but not collapse" characteristic under the ultimate load.

3.3. Load and Deformation. The shear bearing capacity and deformation of the specimens are shown in Table 4. In the table, P_{cr}, P_u, and P_f are the test values of cracking load, limit load, and failure load, respectively; Δ_{cr}, Δ_u, and Δ_f are displacements corresponding to cracking load, limit load, and failure load, respectively; μ denotes the ductility coefficient and $\mu = \Delta_u/\Delta_{cr}$; γ_c, γ_u, and γ_f represent the specimen rotation angle corresponding to cracking load, limit load, and failure load, respectively; K_{cr} and K_u are the increase values of the cracking load and ultimate load of reinforced specimen, respectively, compared with those of the unreinforced specimen with the same aspect ratio, respectively. δ_{cr} and δ_u are the increase values of cracking load and the displacement corresponding to the cracking load of embedded reinforced specimen, compared with those of the unreinforced specimen with the same aspect ratio, respectively.

For JQ1 and JQ2, even after repair and strengthening, there were still cracks in the wall, and thus the cracking load and the displacement were not included in the table. For specimen QA1 with the aspect ratio of 1.8, the cracking load and the ultimate load increased by 8.6% (K_{cr}) and 17.1% (K_u), respectively, compared with those of the unreinforced specimen Q1, while the displacements corresponding to the cracking load and the ultimate load increased by 2.1% (δ_{cr}) and 53.6%, respectively. The ultimate load and the corresponding displacement of specimen JQ1 increased by 6.8% and 47.0%, compared with those of specimen Q1. The ultimate load and the corresponding displacement of specimen QA1 were greater than those of specimen JQ1.

For specimen QA2, the cracking load and ultimate load increased by 6.3% and 12.6%, compared with those of specimen Q2, respectively, while the displacements corresponding to cracking load and ultimate load increased by 5.8% and 17%, respectively. The ultimate load of specimen JQ2 increased by 4.7%, while the displacement

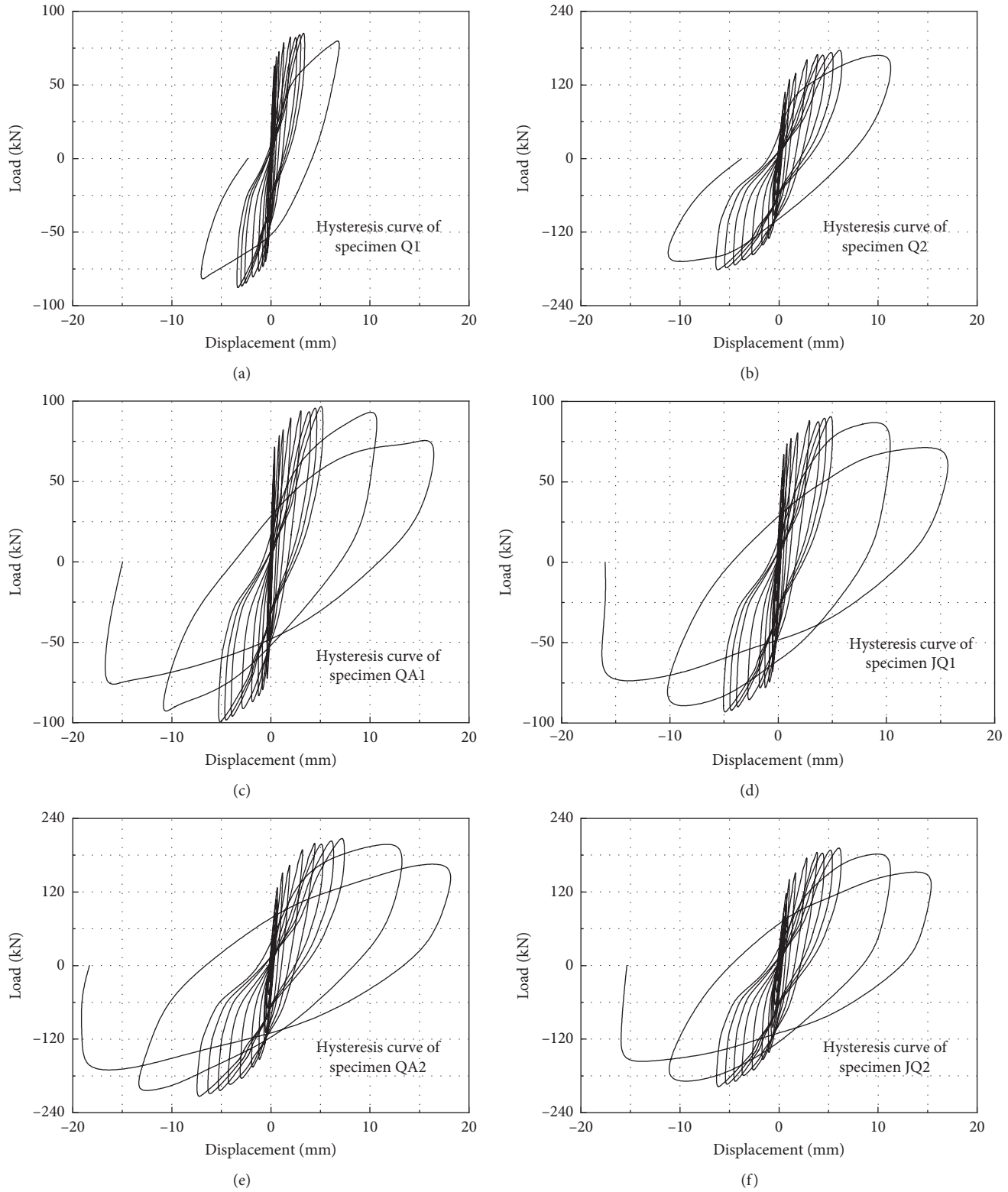

Figure 6: Continued.

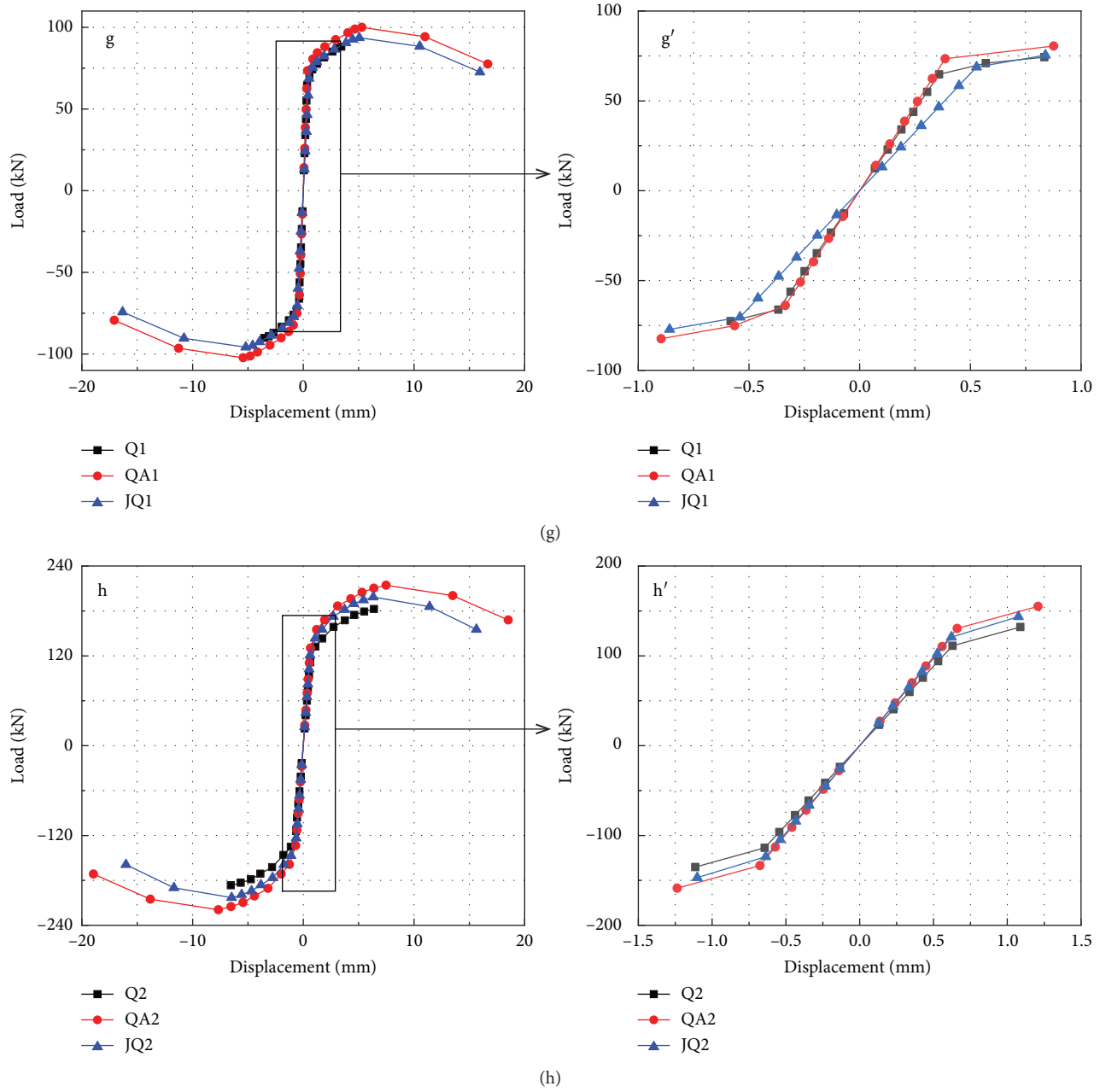

Figure 6: Hysteresis curve and skeleton curve of specimen. (a) Hysteresis curve of specimen Q1. (b) Hysteresis curve of specimen Q2. (c) Hysteresis curve of specimen QA1. (d) Hysteresis curve of specimen JQ1. (e) Hysteresis curve of specimen QA2. (f) Hysteresis curve of specimen JQ2. (g) Skeleton curve of wall with the aspect ratio of 1.8. (g′) Magnification of the skeleton diagrams. (h) Skeleton curve of wall with the aspect ratio of 0.5. (h′) Magnification of the skeleton diagrams.

corresponding to the ultimate load scarcely change compared with that of specimen Q2.

3.4. Hysteresis Curve and Skeleton Curve. The hysteresis curve and the skeleton curve of each specimen are shown in Figure 6. It can be observed that: for specimen Q1 and Q2, the deformation was small during the initial loading stage, and the area encompassed by the hysteresis loop was also small. After cracking, specimen Q1 failed very soon, and the hysteresis loop terminated. For specimen Q2, with the cracks developing, the load increment became smaller, the hysteresis loop area increased gradually, the residual deformation started to increase, and the specimen stiffness began to degenerate. Finally, the hysteresis loop shifted to a horizontal axis, indicating the specimen stiffness decreased rapidly.

For reinforced specimens QA1, QA2, JQ1, and JQ2, the hysteresis curves were similar to those of unreinforced specimens Q1 and Q2 during the initial loading process. After cracks occurred, the hysteresis loop of the reinforced specimens became plumper and encompassed a larger area.

When the ultimate load was reached, the horizontal thrust of the actuator decreased, but the displacement still increased and its increment also increased. A significant descending section occurred in the hysteresis loop until the specimen failed. The hysteresis loops of specimens QA1 and QA2 were plumper and encompassed a larger area than specimens JQ1 and JQ2, respectively, during the stage from cracking to failure.

It can be observed from the skeleton curves that the specimen was basically in the elastic stage before cracking, and the slope (elastic stiffness) of the skeleton curve of each specimen was almost the same in the elastic stage. The specimens QA1 and QA2 had a slightly larger slope, followed by the specimens Q1 and Q2, and the specimens JQ1 and JQ2 had the smallest slope. After cracking, both the masonry and the steel bars participated in bearing the load, and the ultimate bearing capacity of QA1, QA2, JQ1, and JQ2 were improved, compared with that of Q1 and Q2. After reaching the limit load, Q1 and Q2 exhibited significant brittleness and all the reinforced specimens demonstrated good ductility.

3.5. Stiffness Degeneration. The wall stiffness is defined as K_n, which can be calculated according to formula (1).

$$K_n = \frac{\left|+P_n\right| + \left|-P_n\right|}{\left|+\Delta_n\right| + \left|-\Delta_n\right|}, \tag{1}$$

where P_n is the maximum load value of each loading cycle and Δ_n is the displacement value corresponding to the maximum load value. According to formula (1), the stiffness degradation curve of each specimen is shown in Figure 7.

It can be observed from Figure 7 that the initial stiffness of specimen Q1 and QA1 was 130.4 kN/mm and 135.1 kN/mm, respectively, while the initial stiffness of Q2 and QA2 was 195.7 kN/mm and 200.5 kN/mm, respectively, which suggested that the reinforcement itself could not greatly improve the structural stiffness. Hence, the reinforcement would not result in a greater seismic load, which was favorable to the wall. The initial stiffness of JQ1 (125.3 kN/mm) is much close to that of Q1 (130.4 kN/mm), as is the case for JQ2 and Q2 (190.4 kN/mm and 195.7 kN/mm, respectively), which indicated that the initial stiffness of the damaged specimens could be improved by the reinforcement. However, the initial stiffness could not be fully restored, which mainly depended on physical and mechanical properties of the caulking cement and the construction technique.

The stiffness degradation of all the specimens was similar. In the early loading stage, the stiffness degradation rate of the specimens was very large, but later on, it tended to be stable. For the specimens with the aspect ratio of 1.8, when the horizontal displacement reached 3.0 mm, the stiffness was reduced by 75% to 78%; for the specimens with the aspect ratio of 0.5, when the horizontal displacement reached 5.0 mm, the stiffness was reduced by 80%–83%.

3.6. Energy Dissipation Capacity. Energy dissipation value (E) [28] and equivalent viscous damping coefficient (h_e) were used to evaluate the energy dissipation capacity of the specimens, and the calculation formulas are shown in formulas (2) and (3), respectively. In addition, a calculating graph is shown in Figure 8. It is believed that a larger h_e represents a greater energy dissipation capacity. The equivalent viscosity coefficients at the moments of cracking and failure were calculated according to formulas (2) and (3) are listed in Table 5. where S_{ABCD} is the area encompassed by the hysteresis loop curve, while S_{OBE} and S_{ODF} are the areas surrounded by two triangles, respectively.

$$E = S_{ABCD}, \tag{2}$$

$$h_e = \frac{1}{2\pi} \cdot \frac{S_{OBE} + S_{ODF}}{S_{ABCD}}, \tag{3}$$

Before cracking, the energy dissipation capacity of the specimens was very small. For the specimens with the aspect ratio of 1.8, the energy dissipation of QA1 is just 8.3% greater than that of Q1, while for the specimens with the aspect ratio of 0.5, the energy dissipation of QA2 is 16.4% greater than that of Q2. After entering the elastoplastic stage, the energy dissipation ability of the specimens reinforced by embedded steel bars was improved, due to the participation of steel bars in bearing the load (QA1 increased by 252%, compared with Q1, while JQ1 increased by 215%, compared with Q1). Meanwhile, in this stage, with the number of cracks increasing sharply, the damage developed towards a more adequate extent. Besides, the cumulative energy dissipation capacity was also improved. Among the six specimens, the energy dissipation capacity of QA1 and QA2 were the largest, followed by that of JQ1 and JQ2. The energy dissipation capacity of Q1 and Q2 were the smallest. There was a similar law for h_e and E.

4. Conclusions

This paper investigates the seismic performances of unreinforced brick masonry walls, reinforced brick masonry walls, and damaged brick masonry walls strengthened with embedded horizontal steel bars. Based on the analysis, the following findings are obtained:

(1) After the damaged brick masonry walls were reinforced with embedded horizontal steel bars, their ductility could be improved significantly. Because of the constraint of steel bars, these walls exhibited a "crack but not collapse" failure mode under the ultimate load.

(2) For the wall with aspect ratio of 1.8, the ultimate load and the corresponding displacement of specimen JQ1 (damaged and then strengthened) increased by 6.8% and 47.0%, respectively, compared with those of specimen Q1 (unreinforced). For the wall with aspect ratio of 0.5, the ultimate load of JQ2 (damaged and then strengthened) increased by 4.7% than that of specimen Q2 (unreinforced),

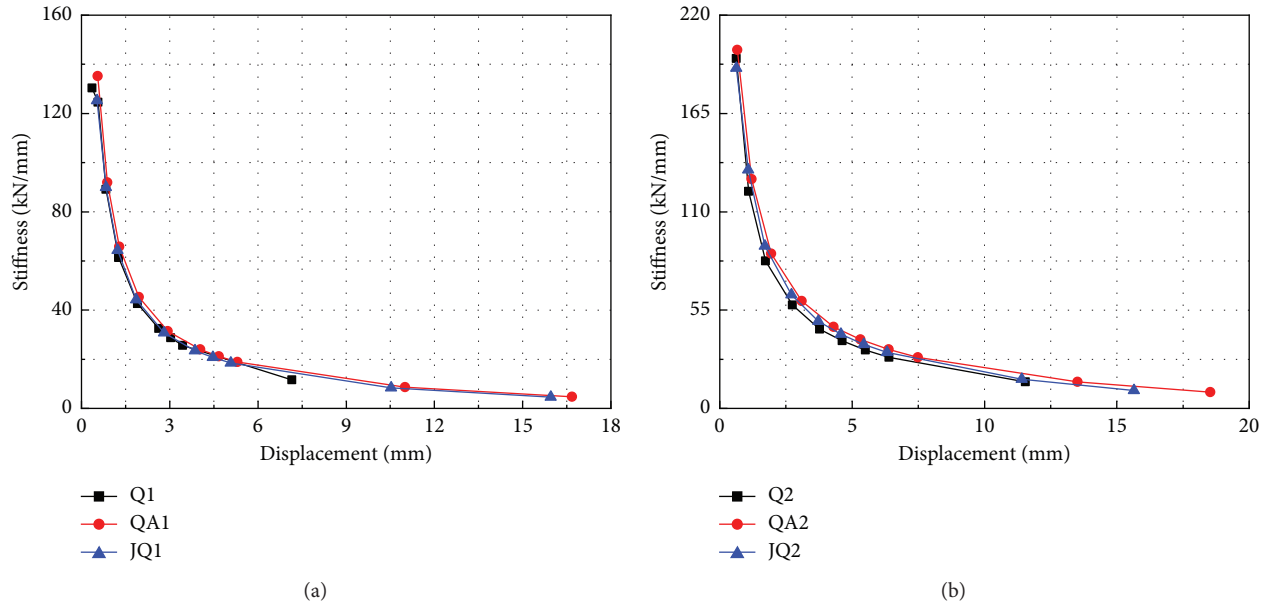

Figure 7: Stiffness degradation curves of specimens. (a) Stiffness degradation curve of wall with aspect ratio of 1.8. (b) Stiffness degradation curve of wall with aspect ratio of 0.5.

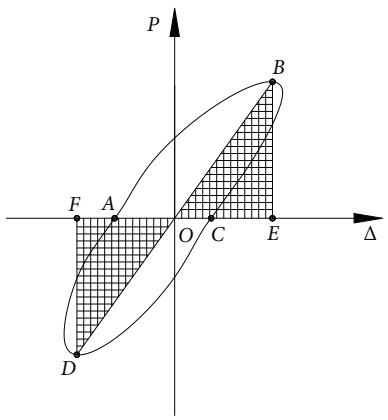

Figure 8: Calculating graph of E and h_e.

Table 5: Energy dissipation capacity of specimens.

Specimen number	Cracking load		Ultimate load	
	E_c (mm^2)	$h_{e,c}$	E_u (mm^2)	$h_{e,u}$
Q1	634.61	0.083	670.04	0.089
QA1	687.18	0.091	2355.58	0.193
JQ1	—	—	2111.51	0.176
Q2	888.61	0.076	1294.31	0.081
QA2	1034.03	0.085	4520.28	0.174
JQ2	—	—	4064.25	0.152

while the displacement corresponding to the ultimate load scarcely increased.

(3) For the walls QA1, QA2 JQ1, and JQ2, their hysteresis curves were similar to those of unreinforced walls Q1 and Q2 during the initial loading process. After cracks occurred, the hysteresis loops of reinforced walls were plumper and encompassed a larger area. When the ultimate load was reached, the horizontal thrust of the actuator decreased, but the displacement still increased and its increment also increased. A significant descending section occurred in the hysteresis loop until the specimen failed. The hysteresis loops of specimens QA1 and QA2 were plumper and encompassed a larger area than specimens JQ1 and JQ2, respectively, during the stage from cracking to failure.

(4) After entering the elastoplastic stage, the energy dissipation capacities of reinforced walls QA1 and QA2 were the strongest, followed by those of QA1 and QA2 (damaged and then reinforced). The energy dissipation capacity of unreinforced walls Q1 and Q2 were the smallest, which was in good agreement with the failure modes of the walls.

(5) The method of embedding horizontal steel bars to reinforce damaged brick masonry walls can effectively improve their seismic performance. This method can be applied in the postseismic reconstruction process.

Data Availability

The data used to support the findings of this study are included within the article.

Disclosure

The opinions expressed in this paper are solely of the authors.

Conflicts of Interest

The authors declare that there are no conflicts of interest regarding the publication of this paper.

Acknowledgments

This work was financially supported by Program for Changjiang Scholars and Innovative Research Team in University (IRT_15R29), the Science and Technology Research Foundation of Gansu (17YF1GA004), and Gansu Civil Engineering Research Institute Co., Ltd. The authors are much grateful to Senior Lecturer Yang Zhiguo for his careful polishing of the manuscript.

References

[1] M. O. Moroni, M. Astroza, and C. Acevedo, "Performance and seismic vulnerability of masonry housing types used in Chile," *Journal of Performance of Constructed Facilities*, vol. 18, no. 3, pp. 173–179, 2004.

[2] B. Zhao, F. Taucer, and T. Rossetto, "Field investigation on the performance of building structures during the 12 May 2008 Wenchuan earthquake in China," *Engineering Structures*, vol. 31, no. 8, pp. 1707–1723, 2009.

[3] S. M. Baldridge and M. Steven, "Performance of structures in the January 2010 MW 7.0 Haiti earthquake," in *Proceedings of the 2011 Structures Congress*, pp. 1660–1671, Las Vegas, NV, USA, April 2011.

[4] K. Stansfield, "Assessing earthquake damage in Haiti," *Structural Engineer*, vol. 88, no. 11, pp. 10–12, 2010.

[5] Y. Pan, X. Wang, R. Guo, and S. Yuan, "Seismic damage assessment of Nepalese cultural heritage building and seismic retrofit strategies: 25 April 2015 Gorkha (Nepal) earthquake," *Engineering Failure Analysis*, vol. 87, pp. 80–95, 2018.

[6] S. Murat, G. Ahmed, and N. Ioan, "Performance of structures in Indonesia during the December 2004 Great Sumatra earthquake and Indian Ocean tsunami," *Earthquake Spectra*, vol. 22, no. 3_suppl, pp. 295–319, 2006.

[7] S. M. Amir and S. M. Reza, "Performance of masonry walls during Kaki, Iran, earthquake of April 9, 2013," *Journal of Performance of Constructed Facilities*, vol. 30, no. 3, Article ID 04015040, 2016.

[8] L. Hofer, P. Zampieri, M. A. Zanini, F. Faleschini, and C. Pellegrino, "Seismic damage survey and empirical fragility curves for churches after the August 24, 2016 Central Italy earthquake," *Soil Dynamics and Earthquake Engineering*, vol. 111, pp. 98–109, 2018.

[9] TMS 402-11/ACI 530-11/ASCE 5-11, *Building Code Requirements for Masonry Structures, (TMS 402-11/ACI 530-11/ASCE 5-11), Masonry Standards Joint Committee*, The Masonry Society, Boulder, CO, USA, 2011.

[10] TEK 12-2B, *Joint Reinforcement for Concrete Masonry*, National Concrete Masonry Association (NCMA), Herndon, VA, USA, 20a05.

[11] GB50702-2011, *Ministry of Housing and Urban-Rural Development of the People's Republic of China (MOHURD). Code for Design of Strengthening Masonry Structures*, China Building Industry Press, Beijing, China, 2011.

[12] D. Zhou, Z. Lei, and J. Wang, "In-plane behavior of seismically damaged masonry walls repaired with external BFRP," *Composite Structures*, vol. 102, pp. 9–19, 2013.

[13] K. M. C. Konthesingha, M. J. Masia, R. B. Petersen, N. Mojsilovic, G. Simundic, and A. W. Page, "Static cyclic in-plane shear response of damaged masonry walls retrofitted with NSM FRP strips-an experimental evaluation," *Engineering Structures*, vol. 50, pp. 126–136, 2013.

[14] N. Reboul, Z. Mesticou, Asi Larbi, and E. Ferrier, "Experimental study of the in-plane cyclic behaviour of masonry walls strengthened by composite materials," *Construction and Building Materials*, vol. 164, pp. 70–83, 2018.

[15] A. I. Cruz O., J. J. Pérez-Gavilán E., and L. Flores C., "Experimental study of in-plane shear strength of confined concrete masonry walls with joint reinforcement," *Engineering Structures*, vol. 182, pp. 213–226, 2019.

[16] A. Triwiyono, A. S. B. Nugroho, A. D. Firstyadi, and F. Ottama, "Flexural strength and ductility of concrete brick masonry wall strengthened using steel reinforcement," *Procedia Engineering*, vol. 125, pp. 940–947, 2015.

[17] F. A. Kariou, S. P. Triantafyllou, D. A. Bournas, and L. N. Koutas, "Out-of-plane response of masonry walls strengthened using textile-mortar system," *Construction and Building Materials*, vol. 165, pp. 769–781, 2018.

[18] S. Bhattacharya, S. Nayak, and S. C. Dutta, "A critical review of retrofitting methods for unreinforced masonry structures," *International Journal of Disaster Risk Reduction*, vol. 7, pp. 51–67, 2014.

[19] M. Corradi, A. D. Schino, A. Borri, and R. Rufini, "A review of the use of stainless steel for masonry repair and reinforcement," *Construction and Building Materials*, vol. 181, pp. 335–346, 2018.

[20] D. Dizhur, M. Griffith, and J. Ingham, "In-plane shear improvement of unreinforced masonry wall panels using NSM CFRP strips," *Journal of Composites for Construction*, vol. 17, no. 6, Article ID 04013010, 2013.

[21] N. Ismail and J. M. Ingham, "In-situ and laboratory based out-of-plane testing of unreinforced clay brick masonry walls strengthened using near surface mounted twisted steel bars," *Construction and Building Materials*, vol. 36, pp. 119–128, 2012.

[22] S. Moreira, L. F. Ramos, B. Csikai, and P. Bastos, "Bond behaviour of twisted stainless steel bars in mortar joints," in *Proceedings of the 9th International Masonry Conference*, Guimaraes, Portugal, July 2014.

[23] R. B. Petersen, N. Ismail, M. J. Masia, and J. M. Ingham, "Finite element modelling of unreinforced masonry shear wallettes strengthened using twisted steel bars," *Construction and Building Materials*, vol. 33, pp. 14–24, 2012.

[24] GB/T 2542-2012, *Test Methods for Wall Bricks*, National Standard of PRC, Beijing, China, 2012.

[25] GB50728-2011, *Technical Code for Safety Appraisal of Engineering Structural Strengthening Materials*, National Standard of PRC, Beijing, China, 2011.

[26] GB1499.1-2008, *Steel for the Reinforcement of Concrete-Part 1: Hot Rolled Plain Bars*, National Standard Of PRC, Beijing, China, 2008.

[27] GB/T. 50129-2011, *Standard for Test Method of Basic Mechanics Properties of Masonry*, National Standard of PRC, Beijing, China, 2011.

[28] JGJ/T 101-2015, *Specification For Seismic Test of Buildings*, Industry Standard of PRC, Beijing, China, 2015.